Effect of laser welding parameters on the microstructure and mechanical properties of dissimilar hastelloy X/Haynes 188 joints

Joël Alexis, Jérémie Graneix, Yannick Balcaen

Dear Author,

Here are the proofs of your article.

- You can submit your corrections **online**, via **e-mail** or by **fax**.
- For **online** submission please insert your corrections in the online correction form. Always indicate the line number to which the correction refers.
- You can also insert your corrections in the proof PDF and **email** the annotated PDF.
- For fax submission, please ensure that your corrections are clearly legible. Use a fine black pen and write the correction in the margin, not too close to the edge of the page.
- Remember to note the **journal title**, **article number**, and **your name** when sending your response via e-mail or fax.
- **Check** the metadata sheet to make sure that the header information, especially author names and the corresponding affiliations are correctly shown.
- **Check** the questions that may have arisen during copy editing and insert your answers/ corrections.
- **Check** that the text is complete and that all figures, tables and their legends are included. Also check the accuracy of special characters, equations, and electronic supplementary material if applicable. If necessary refer to the *Edited manuscript*.
- The publication of inaccurate data such as dosages and units can have serious consequences. Please take particular care that all such details are correct.
- Please **do not** make changes that involve only matters of style. We have generally introduced forms that follow the journal's style.
  Substantial changes in content, e.g., new results, corrected values, title and authorship are not allowed without the approval of the responsible editor. In such a case, please contact the Editorial Office and return his/her consent together with the proof.
- If we do not receive your corrections **within 48 hours**, we will send you a reminder.
- Your article will be published **Online First** approximately one week after receipt of your corrected proofs. This is the **official first publication** citable with the DOI. **Further changes are, therefore, not possible.**
- The **printed version** will follow in a forthcoming issue.

Please note

After online publication, subscribers (personal/institutional) to this journal will have access to the complete article via the DOI using the URL: http://dx.doi.org/[DOI].
If you would like to know when your article has been published online, take advantage of our free alert service. For registration and further information go to: http://www.link.springer.com.

Due to the electronic nature of the procedure, the manuscript and the original figures will only be returned to you on special request. When you return your corrections, please inform us if you would like to have these documents returned.

Metadata of the article that will be visualized in OnlineFirst

ArticleTitle	Effect of Laser Welding Parameters on the Microstructure and Mechanical Properties of Dissimilar Hastelloy X/Haynes 188 Joints	
Article Sub-Title		
Article CopyRight	The Minerals, Metals & Materials Society and ASM International (This will be the copyright line in the final PDF)	
Journal Name	Metallurgical and Materials Transactions A	
Corresponding Author	Family Name	**Alexis**
	Particle	
	Given Name	**Joël**
	Suffix	
	Division	LGP, ENIT/INPT
	Organization	Université de Toulouse
	Address	47 av. d'Azereix, BP1629, 65016, Tarbes cedex, France
	Division	Laboratoire Génie de Production
	Organization	Ecole Nationale d'Ingénieurs de Tarbes
	Address	47 Avenue d'Azereix, BP1629, 65016, Tarbes Cedex, France
	Phone	
	Fax	
	Email	Joel.alexis@enit.fr
	URL	
	ORCID	
Author	Family Name	**Graneix**
	Particle	
	Given Name	**Jérémie**
	Suffix	
	Division	LGP, ENIT/INPT
	Organization	Université de Toulouse
	Address	47 av. d'Azereix, BP1629, 65016, Tarbes cedex, France
	Phone	
	Fax	
	Email	Jeremie.graneix@enit.fr
	URL	
	ORCID	
Author	Family Name	**Balcaen**
	Particle	
	Given Name	**Yannick**
	Suffix	
	Division	LGP, ENIT/INPT
	Organization	Université de Toulouse
	Address	47 av. d'Azereix, BP1629, 65016, Tarbes cedex, France
	Phone	

	Fax	
	Email	Yannick.balcaen@enit.fr
	URL	
	ORCID	

Schedule	Received	10 May 2021
	Revised	
	Accepted	29 August 2021

Abstract	Laser welding is currently a versatile and reliable assembly technique. To save weight in aerostructures and propulsion units and to reduce thermal distortions and the heat-affected zones in these assemblies, autogenous laser welding seems promising. This experimental work addresses dissimilar autogenous laser welding of thin alloy sheets using a Yb:YAG source and a particular optical fibre setting. Hastelloy X and Haynes 188 are the two base metals studied for this assembly. An experimental design allows us to determine the weldability domain. The macro- and microstructure and mechanical properties of the weld seams are investigated. EBSD and EDS analysis revealed microstructural and chemical heterogeneities in the high-power welded seam, but XRD results demonstrated a homogeneous depletion of the carbide density in its fusion zone. Despite such microstructural features, the mechanical properties of Haynes 188 were found to be satisfactory and slightly greater than those of the weaker Hastelloy X.

Footnote Information	Manuscript submitted May 10, 2021; accepted August 29, 2021.

ORIGINAL RESEARCH ARTICLE

Effect of Laser Welding Parameters on the Microstructure and Mechanical Properties of Dissimilar Hastelloy X/Haynes 188 Joints

JOËL ALEXIS, JÉRÉMIE GRANEIX, and YANNICK BALCAEN

Laser welding is currently a versatile and reliable assembly technique. To save weight in aerostructures and propulsion units and to reduce thermal distortions and the heat-affected zones in these assemblies, autogenous laser welding seems promising. This experimental work addresses dissimilar autogenous laser welding of thin alloy sheets using a Yb:YAG source and a particular optical fibre setting. Hastelloy X and Haynes 188 are the two base metals studied for this assembly. An experimental design allows us to determine the weldability domain. The macro- and microstructure and mechanical properties of the weld seams are investigated. EBSD and EDS analysis revealed microstructural and chemical heterogeneities in the high-power welded seam, but XRD results demonstrated a homogeneous depletion of the carbide density in its fusion zone. Despite such microstructural features, the mechanical properties of Haynes 188 were found to be satisfactory and slightly greater than those of the weaker Hastelloy X.

https://doi.org/10.1007/s11661-021-06452-w

I. INTRODUCTION

In jet engines, performance and efficiency are directly related to the combustion temperature. This statement has promoted the constant research and development of new alloys and new thermomechanical routes to produce disks, blades, combustion chambers and exhausts.[1–3] Several superalloys can be associated with optimizing the different parts of the combustion chambers depending on the mechanical and environmental constraints. The nickel-based alloy Hastelloy X is, for example, associated with the Haynes 188 cobalt-based alloy in projected engines. These alloys are commonly assembled by semi-automatic gas tungsten arc welding (GTAW) techniques with filler wires of the same grade as nickel-based superalloys.[4] These welding techniques produce a high thermal distortion due to high energy input. In contrast, the laser welding process induces smaller deformations and can be automated.[5] Moreover, new laser sources, such as disk laser sources, look promising. Currently, disk lasers have a higher power, higher efficiency and higher optical quality than older CO_2 laser sources.[6,7]

JOËL ALEXIS, JEREMIE GRANEIX, and YANNICK BALCAEN are with the Université de Toulouse, LGP, ENIT/INPT, 47 av. d'Azereix, BP1629, 65016 Tarbes cedex, France. JOËL ALEXIS is also with the Laboratoire GVénie de Production, Ecole Nationale d'Ingénieurs de Tarbes, 47 Avenue d'Azereix, BP1629, 65016 Tarbes Cedex, France. Contact e-mail: Joel.alexis@enit.fr.

Manuscript submitted May 10, 2021; accepted August 29, 2021.

The weldability of a superalloy is inversely proportional to the presence of hardening elements. An acceptable level of weldability has been set at maximum levels of 6 pct at. titanium and aluminium.[8] The presence of these chemical elements, which determine the transformations γ/γ' as well as chemical elements other than sulphur or phosphorus,[9] can cause hot cracking by liquation or alternatively embrittlement phenomena after ageing treatment. Liquidation-induced cracks or hot cracks appear at the joints of grains enriched in the solute and are subjected to stress.[10] To improve their weldability, the base metals (BMs) must in particular have a small grain microstructure with no pre-weld heat treatment.[11] It is preferable to weld annealed superalloy sheets and not after a quenching and tempering treatment (final condition before use). The annealed condition is more malleable and allows for better accommodation of cooling-induced deformations during welding. The nature of the grain boundaries also seems to play a role in the weld quality. Special grain boundaries significantly reduce the susceptibility to cracking.[11] Notably, there has been very little documentation regarding the homogeneous Yb:YAG laser welding of the superalloys Hastelloy X and Haynes 188.[12,13] This is even more evident for the heterogeneous welding of these two alloys. The success of dissimilar welds involves the metallurgical compatibility of the BMs and filler metal, similar coefficients of thermal expansion and post-weld heat treatment (PWHT) requirements. Researchers interested in GTAW welds, even CO_2 laser welding of these two alloys, reported some problems of liquation, segregation

Journal : MMTA Dispatch : 6-9-2021 Pages : 11
PIPS No. : 6452 LE TYPESET
MS Code : CP DISK

in the fusion zone (FZ) and the absence of a heat-affected zone (HAZ).[14] The strength of the welds is slightly lower than that of the BM, and their ductility is also weaker. Variations in mechanical properties are noted according to the nature and size of the FZ substructures.[11,12] The most resistant structure seems to be a fine dendritic structure,[13] which is obtained by minimizing the welding energy while maximizing the solidification rate.

It is well known that the control of welding parameters plays a leading role in the welding mode (conduction or keyhole) and the microstructure of the FZ. The purpose of this paper is to highlight the effect of Yb:YAG laser welding process parameters on the dissimilar welding of Hastelloy X and Haynes 188 sheets. The weldability domain of the heterogeneous assembly is presented in the first section as a function of the power density and interaction time. Optimum welding conditions are determined, and the obtained weld seams are analysed. The microstructure of these seams is presented as well as their mechanical properties.

II. EXPERIMENTAL METHODS

A. *Materials*

Hastelloy X nickel-based alloy and Haynes 188 cobalt-based alloy sheets (1.2 mm thick) were used. The plates underwent a solution annealing treatment (1150 °C for 1 hour, water quenching for Hastelloy X; 1475 °C, 1 h, water quenching for Haynes 188). The average grain size was 90 μm for the Hastelloy X sheet (# 4, ASTM E112 standard) and 70 μm for the Haynes 188 sheet (# 4.5, ASTM E112 standard). The chemical compositions and mechanical properties of the materials are given in Tables I and II, respectively.

Table I. Chemical Composition of the Hastelloy X and Haynes 188 Sheets (Wt Pct)

	Ni	Cr	Co	Mo	W	Fe	Mn	Si	C
Hastelloy X	Bal.	22.1 ± 0.45	1.46 ± 0.01	8.74 ± 0.05	0.71 ± 0.01	18.6 ± 0.16	0.60 ± 0.03	0.32 ± 0.007	0.067 ± 0.004
Haynes 188	23.9 ± 0.27	22.1 ± 0.1	Bal.	0.37 ± 0.004	14.1 ± 0.12	2.02 ± 0.02	0.79 ± 0.01	0.30 ± 0.005	0.088 ± 0.001

B. *Laser Welding*

The welds were performed on a TruLaser Cell 3000 machine, which was equipped with a TruDisk Yb:YAG laser source of 3.3 kW and a coaxial optical "2 in 1" fibre (100 μm centre fibre, and 400 μm peripheral fibre).[15] This machine has distinctive features including the ability to dynamically vary the spot diameter at the focal point as well as its position along the optical axis. The Yb:YAG laser beam is generated from a disk, is guided in an optical fibre and is delivered with a near top-hat power density distribution at the focal point. The core fibre (CF) generates a conventional near Gaussian beam profile, and the outer fibre (OF) delivers an annular top-hat power distribution. The use of either fibre configuration provides an adjustable focal diameter of 110 to 370 μm for the CF and 450 to 750 μm for the OF. The focal diameters between 370 and 450 μm are therefore inaccessible.

To limit the number of samples while trying to investigate the influence of multiple parameters of the laser welding process explained above, experimental designs were developed using CORICO software, developed by CORYENT Company. This software provides

Journal : MMTA Dispatch : 6-9-2021 Pages : 11
PIPS No. : 6452 ☐ LE ☐ TYPESET
MS Code : ☐ CP ☐ DISK

Table II. Mechanical Properties of the Hastelloy X and Haynes 188 Sheets

		E (GPa)	YS (MPa)	UTS (MPa)	A (Pct)	HV0.5
Hastelloy X	RD	208 ± 10	446 ± 3	799 ± 2	55 ± 2	230 ± 10
	45°	211 ± 15	446 ± 11	793 ± 11	53 ± 2	
	TD	190 ± 20	456 ± 5	806 ± 5	58 ± 8	
Haynes 188	RD	188 ± 1	524 ± 10	1057 ± 14	76 ± 2	275 ± 11
	45°	200 ± 1	516 ± 4	1048 ± 3	71 ± 2	
	TD	201 ± 1	527 ± 8	1055 ± 7	72 ± 2	

a data analysis tool that allows us to design and process non-orthogonal experimental designs and manage non-linear responses. CORICO software evaluates data by the iconographic correlation method.

The optimal welding parameters were determined using CORICO software based on "desirability" criteria attributed to the geometric criteria described in the standard and to the mechanical properties of the beads such as yield strength and percent elongation. For each response Y, a regression equation is created from the iconographic correlations by CORICO software.

$$Y_I = b_0 + b_1 X_{1i} + \cdots + b_P X_{Pi} + u_i$$

b_p are the coefficients of the partial regression model, the constant u_i is the residue term and the regressors X_{pi} are factors or logical combination of factors correlated to the best answer. From the regression equations, optimisation was performed using also the CORICO software, implementing a Monte Carlo optimisation method. The desirability criterions of this optimisation process are determined on mechanical properties enhancement (both static and fatigue) expected by geometrical features such as a moderately wide weld bead, with very low or no undercut and strictly no underfill. All this procedure is identical to previous work on both alloys, as.[16]

The variable parameters of the different experimental designs are as follows: laser source power P (W), welding head travel speed V (m min^{-1}), gas flow rate D (L min^{-1}), geometrical configuration of the CF or OF beam, and spot diameter at the focal point $\emptyset f$ (μm). The first three parameters are common to all welding processes. The last two parameters are generally associated with the machine configuration. In view of the results of the bibliography, other welding parameters have been fixed, namely, the welding direction corresponds to the rolling direction, the position of the focal point is at -1/3 of the sheet thickness, and the gas shielding towards the weld is argon (20 L min^{-1}). Thirty samples were welded according to the experimental design given for each geometrical configuration. The different weld beads were then observed from metallographic sections to characterize their shape and size. More detailed information is available in a previous publication.[12]

C. *Characterization*

The microstructure of the weld seams was determined from metallographic cross sections obtained with the following preparation procedure: polishing to SiC 4000 grit paper and then polishing to 1/4 μm diamond paste and etching for 2 s with 96 pct HCl and 4 pct H_2O_2 solution. Optical microscopy observations made it possible to determine the weldability domain from the morphologies of the weld seams and their defects. The microstructure of the welds was investigated by optical (PMG3 Olympus), scanning electron microscopy (SEM, JEOL 7000F) and electron backscatter diffraction (EBSD) analyses (Oxford Nordlys Fast camera). The precipitation density and the evolution of the lattice parameter of the solid solution γ were analysed by electron diffraction with transmission electron microscopy (TEM, JEOL JSEM 2100F) and X-ray diffraction (XRD) (line ID15 of the ESRF facility with a wavelength of 0.0142222 nm). The hardness was determined using a ZWICK-ROELL ZHU2.5 instrumented hardness tester at a 500 g load. The tensile tests were carried out using a DEBEN microtensile machine equipped with a 5 kN load cell at a strain rate of 10^{-3} s^{-1} to determine the mechanical behaviour of the produced assemblies.

III. RESULTS AND DISCUSSION

A. *Domain of Weldability*

The weldability domains of the Hastelloy X–Haynes 188 heterogeneous welds are shown in Figure 1 as a function of the power density and interaction time. No cracks in the molten zone or at the interface between molten zone and the heat affected zone were observed by X-ray analysis or by optical observation of metallographic section. Almost all the welds made with the CF exhibited sufficient penetration and a geometry in accordance with the NF L 06 395 2000 standard, but the result is different for the welds made with the OF. Indeed, only a few welds have sufficient penetration and comply with the criteria of the standard. A minimum power density of 10^6 W cm^{-2} and a fluence higher than 5 kJ cm^{-2} are therefore necessary to achieve compliant welds with the OF. The majority of compliant heterogeneous welds are common to the homogeneous welds of both alloys (Figure 2).[12, 13]

Journal : MMTA Dispatch : 6-9-2021 Pages : 11
PIPS No. : 6452 LE TYPESET
MS Code : CP DISK

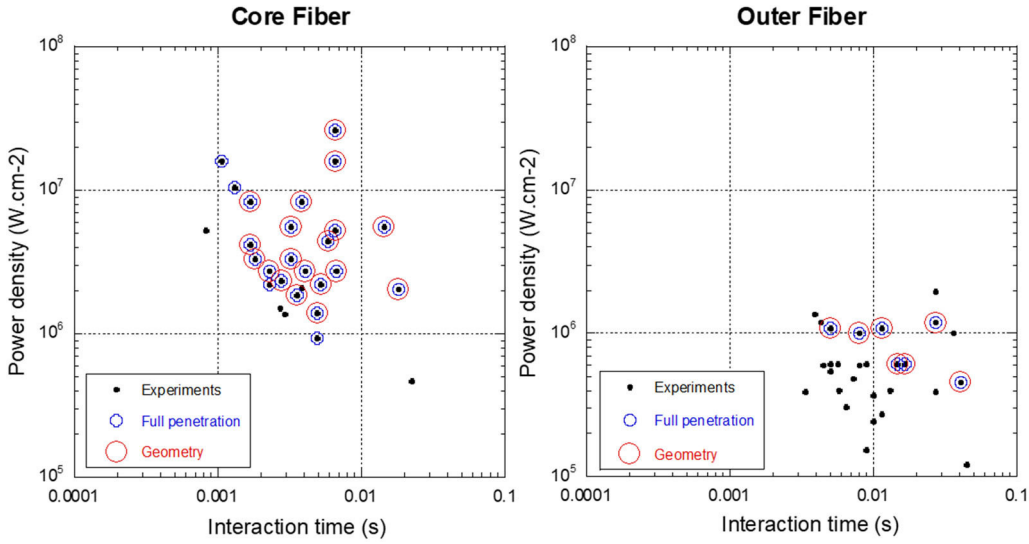

Fig. 1—Weldability domains of the heterogeneous Hastelloy X–Haynes 188 junctions.

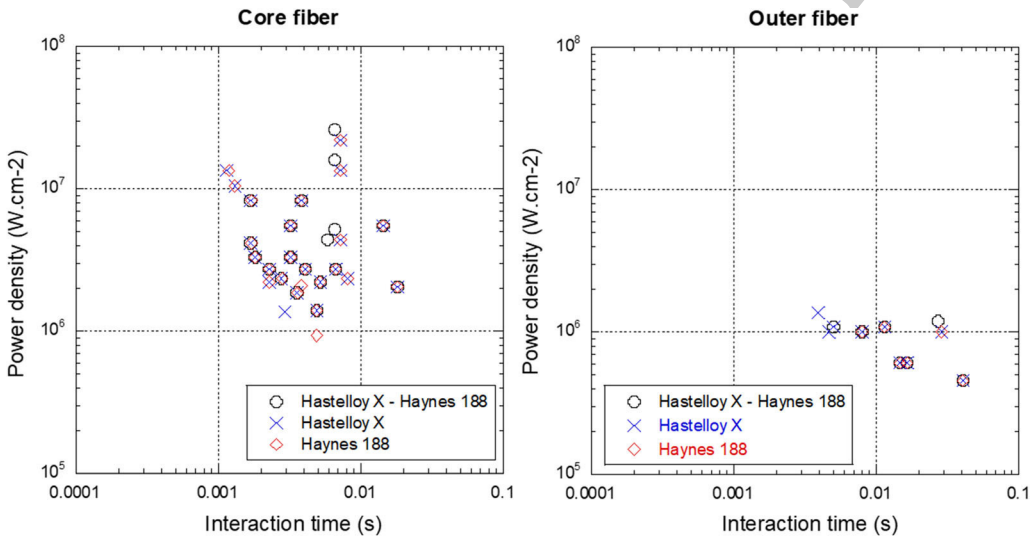

Fig. 2—Weldability domains of the heterogeneous Hastelloy X–Haynes 188 junctions and Hastelloy X or Haynes 188 junctions.

The welding conditions optimized to obtain sufficient penetration and bead geometry that comply with the abovementioned standard were determined using CORICO software from CORYENT. The optimal processing conditions are given in Table III.

B. *Microstructure of the Optimized Welds*

SEM micrographic cross sections of the obtained weld seams are presented in Figure 3(a) and (b). The optimized heterogeneous bead obtained with the core fibre has well-defined interfaces between the BM and the FZ. Contrary to what was observed for the homogeneous assemblies,[12] no cracks were found on this heterogeneous weld bead. This result can be induced by the low welding speed implemented (1 mm min^{-1}). The alloys studied, particularly Hastelloy X, are susceptible to liquation-induced hot stress cracking. A low welding rate leads to a decrease in cooling rate during solidification and consequently a decrease in thermal stresses.[17, 18] The filling of liquefied grain boundaries is also proposed as factor contributing to the prevention or reduction of hot cracking especially in laser welding of Hastelloy X.

Some grain boundaries close to the melted zone are marked, particularly on the Hastelloy X side. Liquation zones are observable (Figure 3(c)). These different analyses also remain true for welds made with the OF. The presence of cellular growth and dendritic zones was determined from micrographic observations at a higher magnification. Typical micrographs are shown in Figure 3(d) to (f). The proportion of dendritic zones is very important in the Hastelloy X/Haynes 188 core fibre weld seam. The cellular zone represents only a 150 μm

Journal : MMTA Dispatch : 6-9-2021 Pages : 11
PIPS No. : 6452 LE TYPESET
MS Code : CP DISK

thick border at the BM-FZ interface. This result is not the same for the Hastelloy X/Haynes 188 weld obtained by the OF since the proportions of dendritic and cellular zones tend to be equal. This last weld is formed of a broad cellular area close to the BM and a dendritic zone in its centre.

SEM backscattered electron observations revealed chemical contrasts in the FZ (Figure 4(a), (b)), confirmed by energy dispersive spectroscopy (EDS) analyses. The chemical composition of the CF bead FZ appears to be relatively homogeneous at a macroscopic scale (Figure 4(d), (f)). EDS profiles confirm this statement in the centre of the cords. Only slight variations (approximately 2 to 3 pct) are detected over 100 μm distances. On the other hand, significant macrosegregations are observed in the Hastelloy X/Hayne 188–OF cords (Figure 4(c) and (e)). Some areas of the melted zone present high concentrations of nickel and molybdenum, a major alloying element of Hastelloy X, and other areas are cobalt and tungsten rich, typically originating from Haynes 188. These global analyses were supplemented by local analyses, which showed a slight increase in the chromium, molybdenum and tungsten contents in the interdendritic zones.

Table III. Processing Parameter Values for Optimized Welds According to Criteria Based on the Standard NF L 06 395 2000

	Core Fibre	Outer Fibre
Power (W)	765	2330
Welding Speed (m min^{-1})	1	4.62
Spot Size (μm)	203	527
Face Argon Flow (l min^{-1})	35	40
Power Density (kW cm^{-2})	2363	1277
Fluence (kJ cm^{-2})	28.8	8.7

The evolution of the ratio of the thermal gradient to the solidification rate (G/R) explains the microstructural changes in the fusion zone. The microstructure of the weld can progressively change from a planar solidification mode at the interface of the weld (maximum G/R), to a cellular mode and then to a dendritic mode in the central region of the FZ due to the decrease of G/R towards the centerline of the FZ. On one hand, the CF-obtained seam presents an homogeneous distribution of chemical species, and a dendritic structure. This could indicate a moderate solidification time and an enhanced expression of constitutional supercooling. On the other hand, the weld seam obtained with OF, high power setting and quite high welding speed, presents a heterogeneous distribution of solute (Figure 4(e)). The discontinuous nature of metal-weld solidification produces the formation of solute bands within the weld. The growth rate fluctuates cyclically above and below a mean value which is a function of the welding speed. Correlated to the presence of a thicker cellular zone, exposed at Figure 3(b), it could be related to a higher solidification rate, and steeper thermal gradient, limiting the abovementioned phenomenon.

The microstructures observed for the heterogeneous bead obtained with the CF are very similar to those of the homogeneous cords (Figure 5).[10] The solidification of the FZ begins with epitaxial growth from partially melted grains. This zone obeys a cellular growth mode. Then, the growth of some favourably oriented grains, presenting (100) to the joint plane, appears. The welding

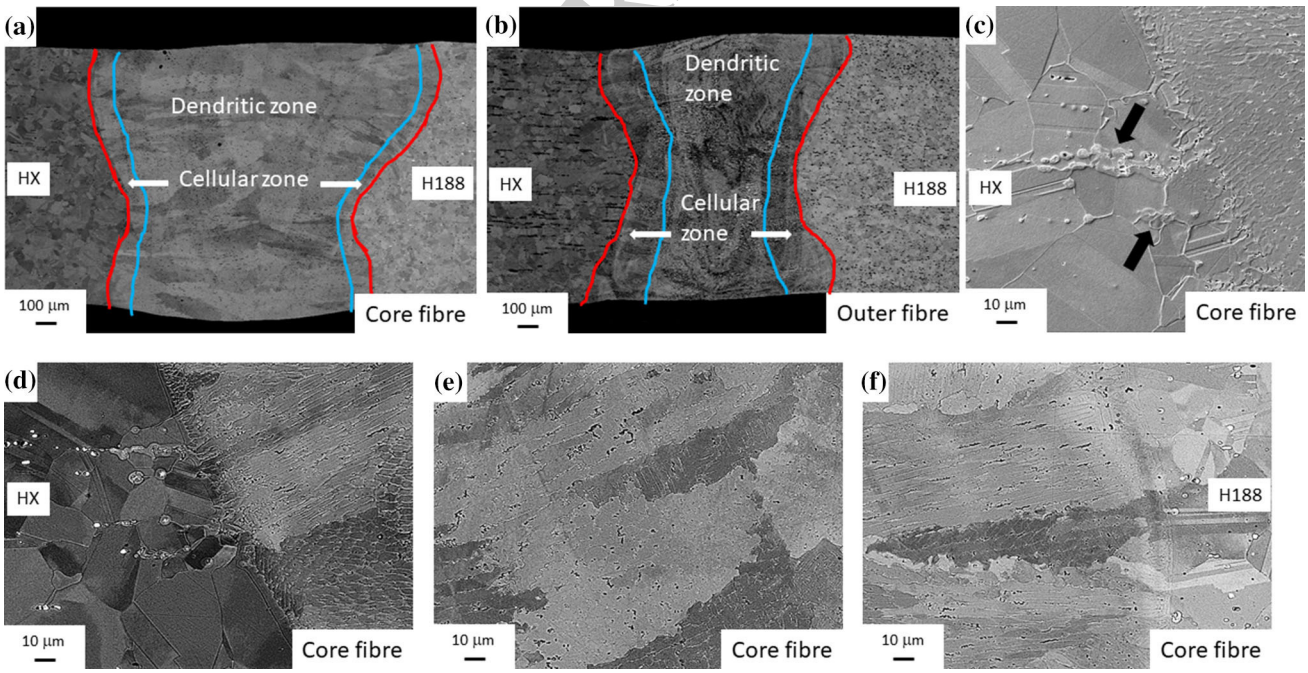

Fig. 3—Cross-sectional observations of the optimized weld by scanning electron microscopy. (*a*, *b*) Overall observation and (*c*, *d*) observation of the fusion zone–Hastelloy X interface..

Journal : MMTA Dispatch : 6-9-2021 Pages : 11
PIPS No. : 6452 ☐ LE ☐ TYPESET
MS Code : ☐ CP ☐ DISK

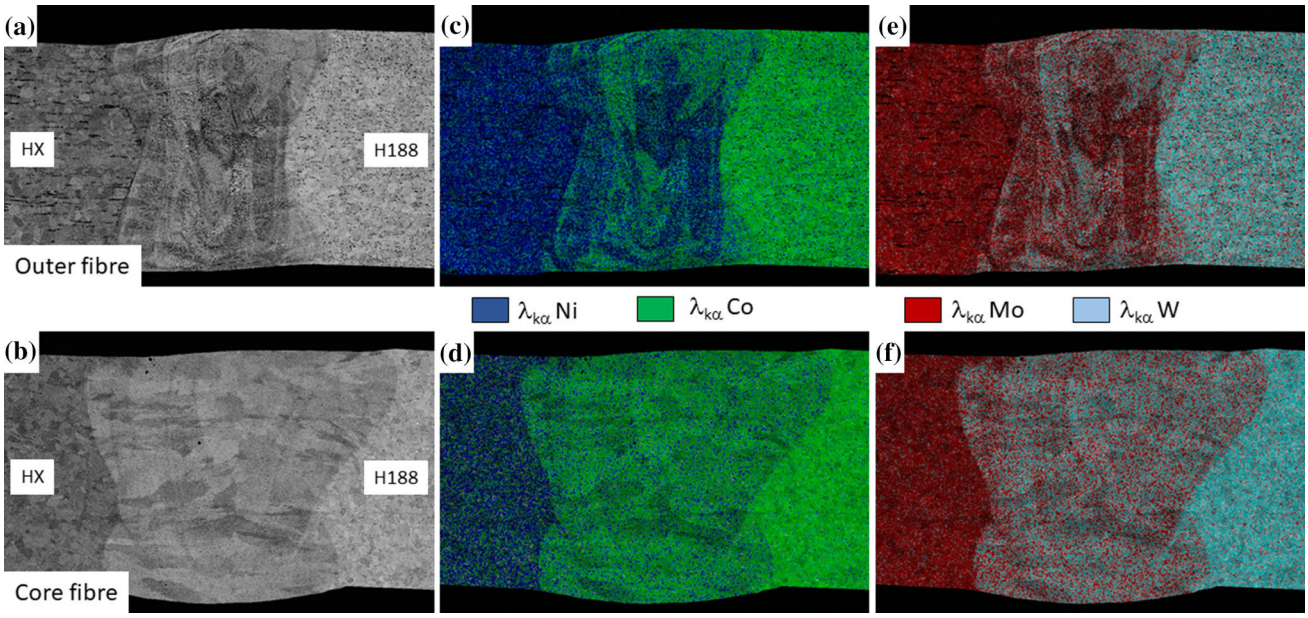

Fig. 4—EDS mappings made in the TD-ND plane of the heterogeneous assemblies of Hastelloy X/Haynes 188. Optimized welds obtained by (*a*, *c*, *e*) outer fibre and (*b*, *d*, *f*) core fibre..

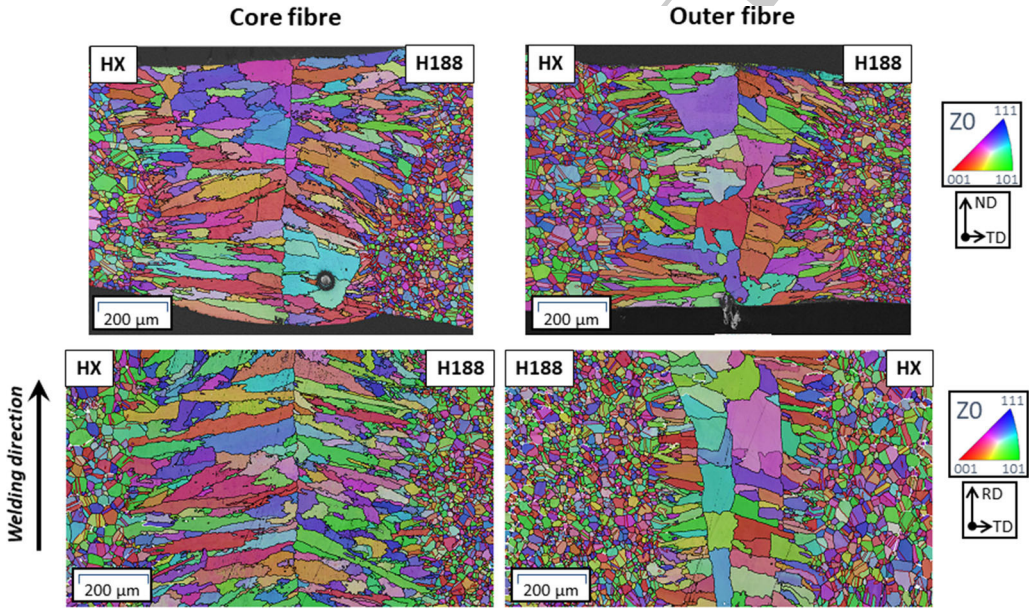

Fig. 5—IPF Z_0 coded EBSD cartographies of the optimized welded seams of the heterogeneous Hastelloy X/Haynes 188 assemblies, on the cross sections (top) and longitudinal sections 400 μm above the median plane of the sheet (bottom)..

speed seems sufficiently important to extend the melt pool backwards; the grains then develop in the direction of the higher temperature gradient. The OF weld microstructures are significantly different. A columnar zone consisting of epitaxially grown grains remains. However, the width of this area is very limited. On the other hand, large odd-shaped grains are observed in the centre of the weld. The joint plane is then more diffuse in this cord. Comparing data displayed on Figures 3(b) and 4(c) and 5 top right, it seems that odd-shaped grains appearance is correlated to dendritic microstructure in poorly-mixed solute areas. These microstructural evolutions have not been demonstrated in homogeneous seams, even if some optimized homogenous assemblies have been developed with very close processing parameters. The possible explanation of this particular microstructure could be related to the poor mixing of the chemical species in the weld pool, leading to steep chemical gradients in it, promoting such heterogeneous nucleation.

Journal : MMTA Dispatch : 6-9-2021 Pages : 11
PIPS No. : 6452 ☐ LE ☐ TYPESET
MS Code : ☐ CP ☐ DISK

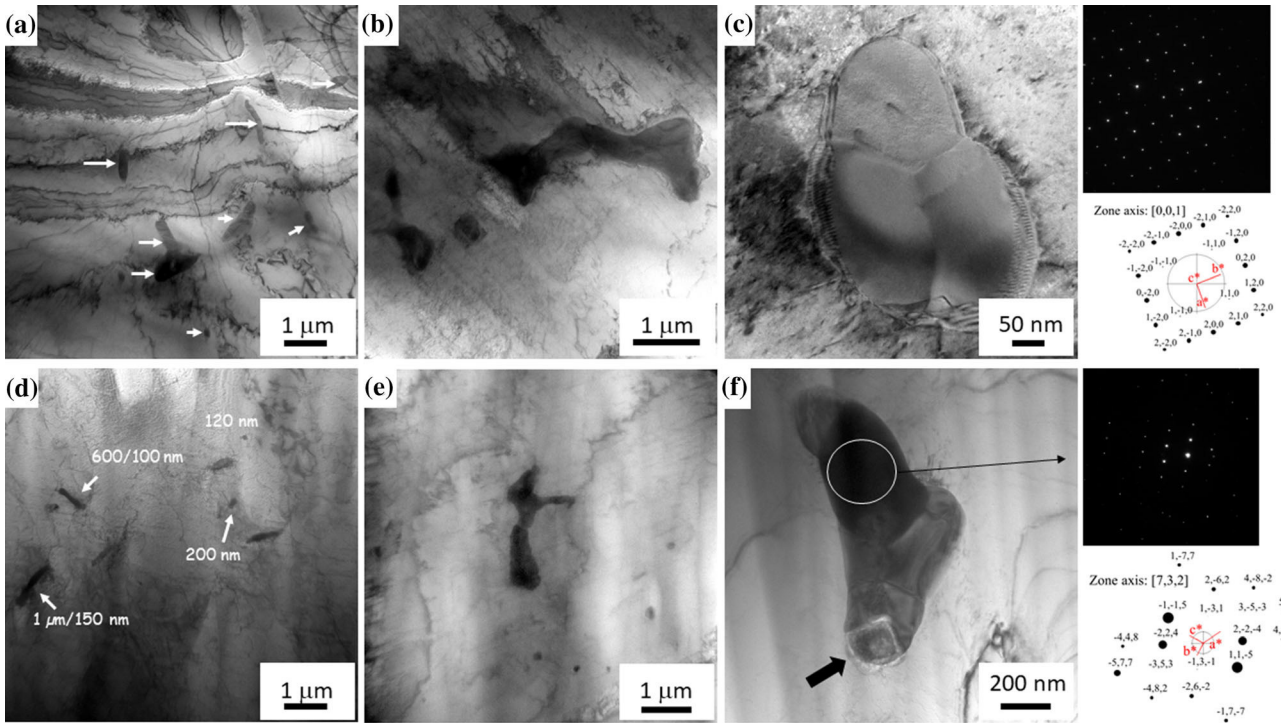

Fig. 6—MET observations of the precipitates present in the weld bead obtained with the (*a* to *c*) CF and (*d* to *f*) OF. The (c) sigma phase precipitate and (f) M_6C carbide. Indexing of the diffraction patterns with Carine software..

The shape and size of the particles in FZs are highly variable (Figure 6(a) to (f)). In addition, these particles differ from those observed in the two reference alloys. Their shape in FZs can be characterized as tortuous and very rounded. The particles whose sizes were less than 500 nm in the Haynes 188 alloy had an angular shape, and the larger particles were rounded. For the Hastelloy X alloy, particles below 500 nm were rounded. The structure of some particles was determined by diffraction. The selected area diffraction pattern of the oriented particles, presented in Figure 6(c), can be indexed according to the [001] zone axis of the tetragonal σ phase (P42/mnm space group, lattice parameters a = 0.91 nm and c = 0.48 nm). Figure 6(f) shows the pattern obtained for one of the observed carbides. The 0.40 nm inter-reticular distance corresponds to the (220) planes of the face-centred cubic (FCC) M_6C carbide. To confirm the nature of the M_6C carbides, several zone axis were analysed on some particles (Figure 7).

In the melted zone of the OF seams, EDS analysis highlighted two typical particles: carbides, identified as M_6C, and lanthanum-rich particles (Table IV). The M_6C particles generally surround the lanthanum-rich particles (Figure 6(f)). Regarding the particles in the FZ of the CF, three typical compositions are highlighted: σ-phase particles, M_6C carbides and lanthanum-rich particles. The chemical composition of the M_6C carbides present in the molten zone whatever the fiber used (CF or OF) is different from that of the carbides analyzed in each alloy. They contain both Molybdenum and Tungsten. In addition, lanthanum-rich particles are not detected in the base alloys. The precipitation of these second phases (M_6C, σ) in the interdendritic zones have already been observed by many authors.[19, 20] A. Ghasemi et al. show that the M_6C and σ phases appear at the end of solidification of Hastelloy X alloy between 1315 and 1280 °C due to the segregation of chromium and molybdenum and not during a solid state transformation during cooling.[21]

The evolution of the precipitate densities in the FZ was determined via X-ray analysis by the evolution of the M_6C (422) peak intensity in the FZ compared to the same peak in the BM (Figure 8). The X-ray probe spot was assimilated to a 100 μm diameter disk, scanning the total width of the seam from the BM to BM through the sheet thickness. Superimposing the geometry of the cords on these data, the intensity ratio does not change identically with respect to the two CF and OF cords (Figure 9). With the CF, the population of M_6C precipitates decreases progressively from the BM to the centre of the FZ. Therefore, there appears to be a precipitate density gradient within the FZ. The width of the zone containing a very small proportion of M_6C carbide in the centre of the FZ for the CF condition corresponds approximatively to the width of the laser beam for a power density greater than 10^6 W cm^{-2}. The dissolution seems more important in this area. For OF welding, this progressive evolution disappears, and the peak relative intensity remains constant in the FZ at the 20 pct level. These results are comparable to those of the Haynes 188 homogeneous assemblies.[12]

The lattice parameter of the solid solution in the FZ is different from that of the nickel-rich solid solution (Hastelloy X) or cobalt-rich solid solution (Haynes 188) (Figure 10). At the centre of the welds, an intermediate

Journal : MMTA Dispatch : 6-9-2021 Pages : 11
PIPS No. : 6452 ☐ LE ☐ TYPESET
MS Code : ☐ CP ☐ DISK

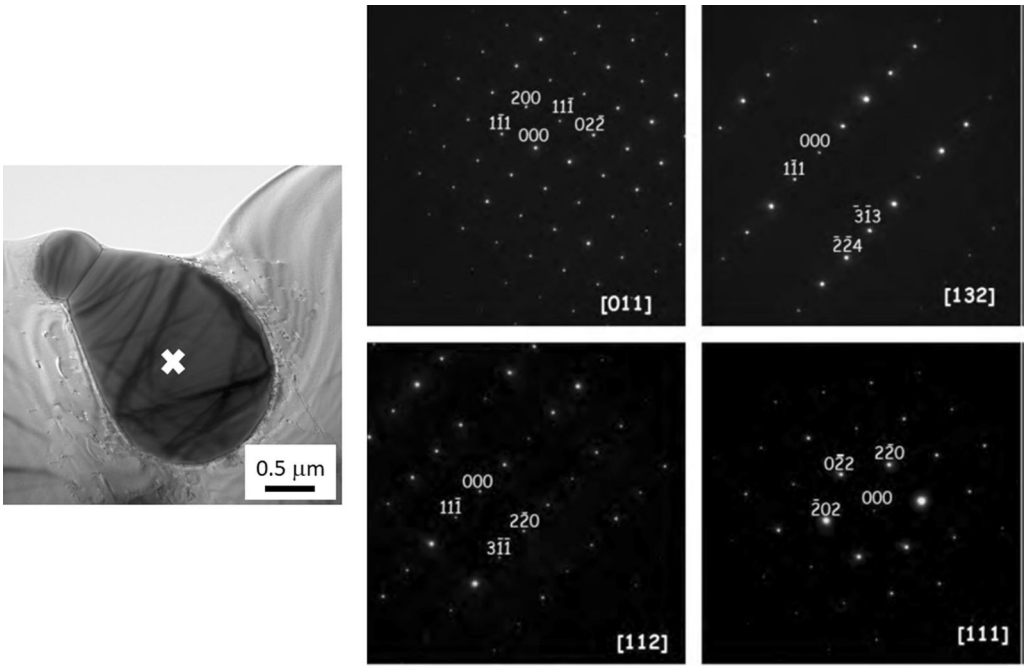

Fig. 7—Electron diffraction patterns of an M_6C carbide for four different zone axis orientations [011] [111] [112] and [132]..

Table IV. Chemical Composition of Particles Observed in Alloys and Welds

Atomic Percent	Cr	Ni	Co	Fe	Mo	W	La
M_6C Carbide (Hastelloy X Alloy)	27	26	—	10	35-37	1	—
M_6C Carbide (Haynes Alloy)	27-28	11-15	23-28	1	0.5-1	29-33	—
M_6C Carbide (OF Weld)	35-40	17-23	10-19	6-8	10-18	5	—
M_6C Carbide (CF Weld)	43	16	16	7	18	6	—
σ Phase (CF Weld)	33	29	15	9.5	9	4	—
Lanthanum-Rich Precipitates (OF and CF Welds)	6–18	4–23	3–10	1–7	2–5	0–1	36–83

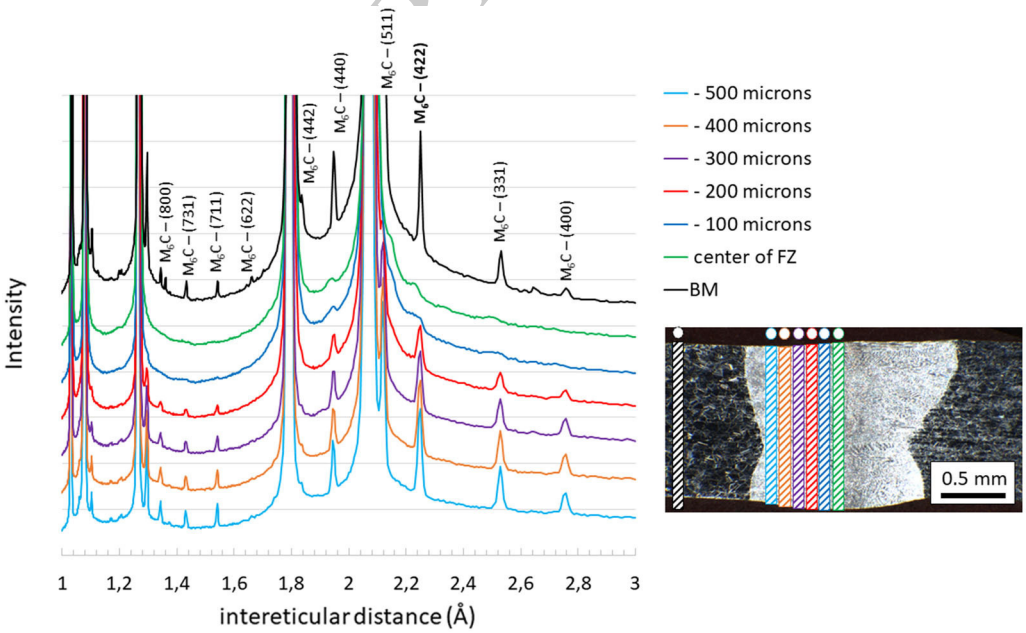

Fig. 8—Superimposed X-rays diffractograms obtained through weld seam.

Journal : MMTA Dispatch : 6-9-2021 Pages : 11
PIPS No. : 6452 ☐ LE ☐ TYPESET
MS Code : ☐ CP ☐ DISK

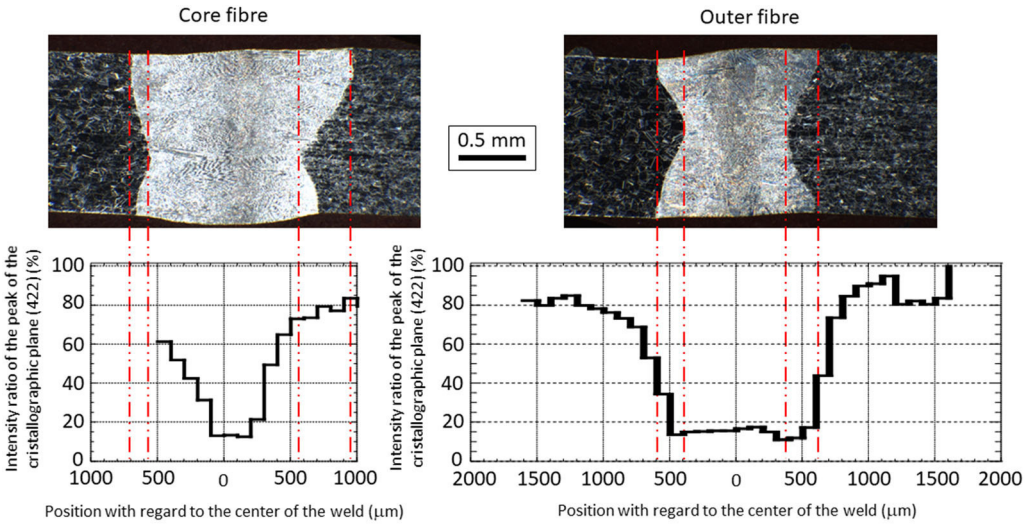

Fig. 9—Location of the X-ray diffraction analysis of the Hastelloy X–Haynes 188 welds obtained in the CF and OF (top). Diffraction intensity ratio by the (422) planes of the M_6C precipitates in the weld with respect to the base metal..

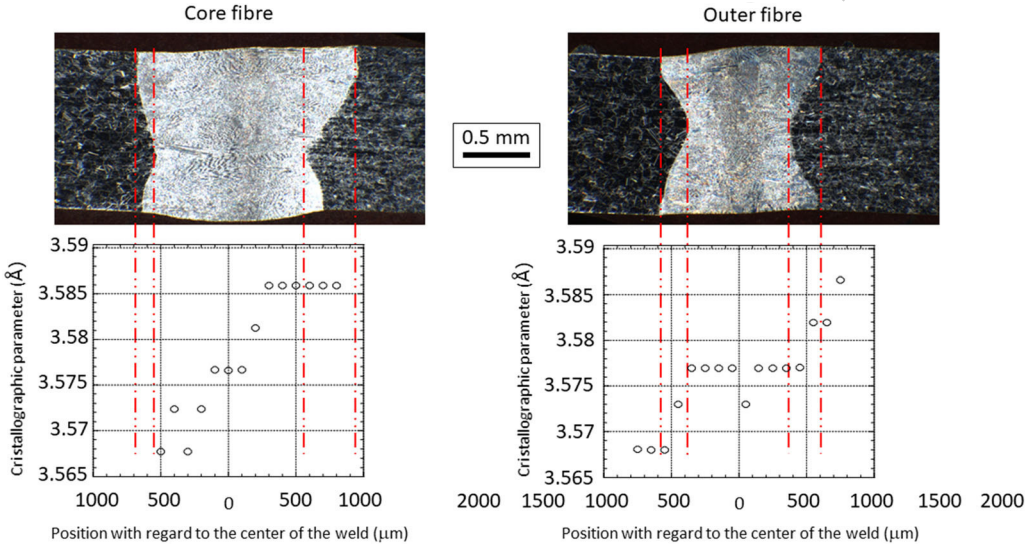

Fig. 10—Evolution of the FCC solid solution lattice parameter..

value is taken because of the interdiffusion phenomena between Ni and Co in the bead.

C. *Mechanical Properties of the Optimized Welds*

The mechanical behaviour of the welded specimens is explored through tensile tests, and the results are presented in (Figure 11). The tensile behaviour is intermediate between the two BMs. The mechanical strength of the welded specimens, regardless of the selected fibre, is actually close to that of the Hastelloy X alloy (Table V). A slight reduction in the ductility is recorded for the CF welds compared to the OF welds. The fractures of all the specimens are localized in the Hastelloy X BM, several millimetres from the FZ. This finding explains the values of the mechanical properties of the heterogeneous weld seams solicited in transverse directions. The mechanical strength of these welded specimens is in fact conditioned by the maximum strength of the weaker Hastelloy X. The slight difference in the ductility recorded is explained by a purely geometric effect (different width of the welds depending on the type of fibre compared to the length of the useful zone). The mechanical properties of the welds (FZ and HAZ) were determined using tensile specimens extracted in the FZ along the welding direction (Figure 9). The results obtained for the welds confirm the first results in the transverse direction. The mechanical properties of

Journal : MMTA Dispatch : 6-9-2021 Pages : 11
PIPS No. : 6452 LE TYPESET
MS Code : CP DISK

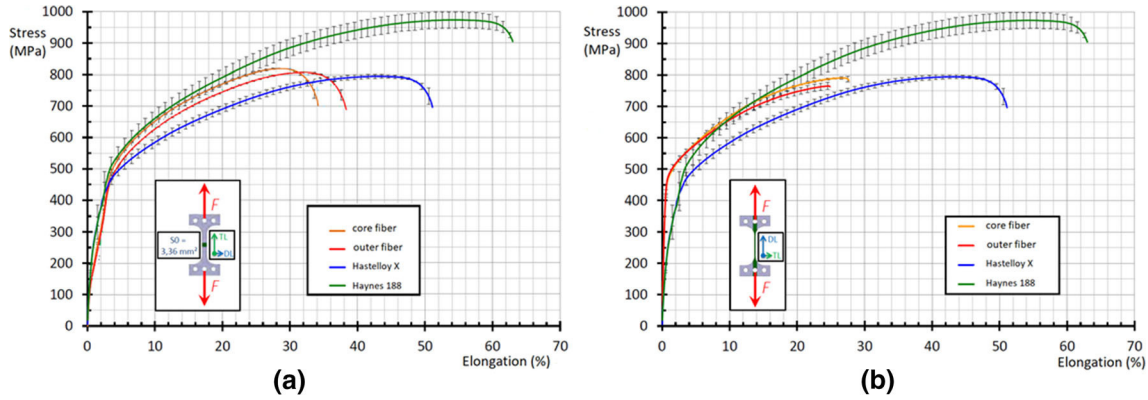

Fig. 11—Tensile tests performed on heterogeneous and homogeneous welds in the transverse direction (*a*) and welding direction (*b*)..

Table V. Mechanical Properties of Heterogeneous Assemblies Hastelloy X/Haynes 188 (Tensile Tests in the Transverse Direction)

Test Direction		UTS (MPa)	Elongation (Pct)	Fracture Localization
	Hastelloy X	795 ± 8	48 ± 0.1	—
	Haynes 188	974 ± 36	57 ± 1.7	—
Transverse Welding Direction	core fibre	819 ± 2	29 ± 0.6	Hastelloy X BM
Transverse Welding Direction	outer fibre	807 ± 2	33 ± 0.3	Hastelloy X BM
Welding Direction	core fibre	792 ± 4	29 ± 1.6	—
Welding Direction	outer fibre	767 ± 13	25 ± 1.6	—

the fused zone solicited in the welding direction for the Hastelloy X/Haynes 188 heterogeneous welds are close to those of the Hastelloy X welds (Table V).

IV. CONCLUSION

Two different optima were determined for each type of fibre, essentially based on geometrical defect reduction. Both optimums produce power densities above 10^6 W.cm^2 but very different fluence levels, leading to a counter-intuitive wider FZ for the CF weld seam than for the OF weld seam. The obtained weld seams are sound, with weak liquations. The microstructure of the FZ consists of a fine cellular growth zone, which evolves dendritically in the centre of the FZ. The width of the cellular zone is more important in the selected OF welding condition due to the high welding speed and low fluence levels, leading to a high solidification factor G/R. This high solidification rate is also confirmed by the poor solute mixing evidenced by EDX analysis of the OF weld seam. This behaviour could be the origin of the odd-shaped dendritic grains in the centre of the FZ, highlighted in EBSD analysis. Secondary phases, such as carbides, were found to be strongly and homogeneously diluted in this seam, contrary to the CF weld seam, in which the carbide density diminished progressively from the BM to the centre of the FZ. However, the mechanical properties remain satisfactory, and fractures occur in the weaker Hastelloy X.

ACKNOWLEDGMENTS

The authors are thankful to EXAMECA for their financial support, in particular for providing the Haynes 188 and Hastelloy X alloys. Furthermore, we wish to thank Cédric Bellot, Director of ACRDM, for giving our team access to the ~~ACRDM synchrotron facilities~~ at ESRF and Marie-Christine Laffont, CIRIMAT, for TEM observations.

CONFLICT OF INTEREST

On behalf of all authors, the corresponding author states that there is no conflict of interest.

REFERENCES

1. N. Rao: Advances in Gas Turbine Technology, InTechOpen, 2011, 13.
2. T.M. Pollock: *Nat. Mater.*, 2016, vol. 15, pp. 809–815.
3. A. Devaux, E. Georges, and P. Héritier: *Adv. Mater. Res.*, 2011, vol. 278, pp. 405–410.
4. M. Sathishkumar and M. Manikandan: *J. Mater. Eng. Perform.*, 2020, vol. 29, pp. 5395–5408.
5. F. Zapirain, F. Zubiri, F. Garciandía, I. Tolosa, S. Chueca, and A. Goiria: *Phys. Procedia*, 2011, vol. 12, pp. 105–112.
6. A. Giesen and J. Speiser: *IEEE J. Sel. Top. Quantum Electron.*, 2007, vol. 13, pp. 598–609.
7. G. Verhaeghe and B. Dance: *International Congress on Applications of Lasers & Electro-Optics*, Temecula, California, USA, Laser Institute of America, 2008, p. 710.

Journal : MMTA Dispatch : 6-9-2021 Pages : 11
PIPS No. : 6452 ☐ LE ☐ TYPESET
MS Code : ☐ CP ☐ DISK

8. ASM International, ed., ASM handbook, 10th editon, ASM International, Materials Park, Ohio, 1990.
9. J.N. DuPont, J.C. Lippold, S.D. Kiser: Welding Metallurgy and Weldability of Nickel-base Alloys, (n.d.) 456.
10. P. von Witzendorff, S. Kaierle, O. Suttmann, and L. Overmeyer: *Metall. Mater. Trans. A*, 2015, vol. 46A, pp. 1678–1688.
11. E.M. Lehockey, G. Palumbo, and P. Lin: *Metall. Mater. Trans. A*, 1998, vol. 29A, pp. 3069–3079.
12. J. Graneix, J-.D. Beguin, J. Alexis, and T. Masri: *Metall. Mater. Trans. B*, 2017, vol. 48B, pp. 2007–2016.
13. J. Graneix, J.D. Beguin, J. Alexis, and T. Masri: *Adv. Mater. Res.*, 2015, vol. 1099, pp. 61–70.
14. J. Hofweber, N.F. Fiore, and W.T. Ebihara: *Mater. Sci. Eng.*, 1977, vol. 27, pp. 157–162.
15. W. Andreasch, R. Huber, and D. Mock: *Laser Tech. J.*, 2011, vol. 8, pp. 38–41.
16. J. Graneix, J-.D. Beguin, F. Pardheillan, J. Alexis, and T. Masri: *MATEC Web Conf.*, 2014, vol. 14, p. 13006.
17. J.J. Pepe and W.F. Savage: *Weld. J.*, 1970, vol. 49 (12), pp. 545s–553s.
18. M. Pakniat, F. Malek Ghaini, and M.J. Torkamany: *Mater. Des.*, 2016, vol. 106, pp. 177–183.
19. R. Sihotang, P. Sung-Sang, and B. Eung-Ryul: *Mater. Res. Innov.*, 2014, vol. 18 (sup2), pp. S2-1074–S2-1080.
20. J. Lippold, J. Sowards, G. Murray, B. Alexandrov, and A. Ramirez: *Hot Cracking Phenomena in Welds II*, Springer, New York, 2008, pp. 147–170.
21. A. Ghasemi, A. Mohammad Kolagar, and M. Pouranvari: *Mater. Sci. Eng. A*, 2020, vol. 793, p. 139861.

Journal : MMTA Dispatch : 6-9-2021 Pages : 11
PIPS No. : 6452 ☐ LE ☐ TYPESET
MS Code : ☐ CP ☐ DISK